



This is a repository copy of *Modelling and vector control of dual three-phase PMSM with one-phase open*.

White Rose Research Online URL for this paper:
<https://eprints.whiterose.ac.uk/175419/>

Version: Published Version

Article:

Hu, Y., Zhu, Z.Q. orcid.org/0000-0001-7175-3307 and Wu, Z. (2021) Modelling and vector control of dual three-phase PMSM with one-phase open. IET Electric Power Applications, 15 (7). pp. 847-860. ISSN 1751-8660

<https://doi.org/10.1049/elp2.12064>

Reuse

This article is distributed under the terms of the Creative Commons Attribution (CC BY) licence. This licence allows you to distribute, remix, tweak, and build upon the work, even commercially, as long as you credit the authors for the original work. More information and the full terms of the licence here:
<https://creativecommons.org/licenses/>

Takedown

If you consider content in White Rose Research Online to be in breach of UK law, please notify us by emailing eprints@whiterose.ac.uk including the URL of the record and the reason for the withdrawal request.



eprints@whiterose.ac.uk
<https://eprints.whiterose.ac.uk/>

Modelling and vector control of dual three-phase PMSM with one-phase open

Yashan Hu¹  | Z. Q. Zhu² | Zhan-yuan Wu³

¹College of Electrical and Information Engineering, Hunan University, Changsha, Hunan, China

²Department of Electronic and Electrical Engineering, University of Sheffield, Sheffield, UK

³Siemens Gamesa Renewable Energy Limited, Sheffield, UK

Correspondence

Yashan Hu, College of Electrical and Information Engineering, Hunan University, Changsha, Hunan, China.

Email: hu_ya_shan@sina.com

Funding information

Huxiang High-Level Talent Gathering Project of HUNAN Province, Grant/Award Number: 2019RS1013; Natural Science Foundation of Hunan Province, China, Grant/Award Number: 2020JJ4006

Abstract

This study proposes a generic mathematical modelling and decoupling fault-tolerant vector control for dual three-phase permanent magnet synchronous machine (PMSM) with one phase open based on the conventional dual three-phase voltage source inverters, accounting for the mutual coupling between two sets of three-phase windings and the second harmonic inductance. When the dual three-phase PMSM has one phase open, the permanent flux-linkages are asymmetric and there are second harmonic components in the conventional synchronous reference frame (dq -frame). Based on the proposed mathematical modelling, both permanent magnet flux-linkages and currents become DC values in the dq -frame, and therefore, the conventional proportional integral (PI) controller can be used to regulate the dq -axis currents. Then, a decoupling fault-tolerant vector control with/without a dedicated feed-forward compensation is proposed to validate the correctness of the proposed mathematical modelling. Experimental results on a prototype dual three-phase PMSM with one phase open show that the second harmonic dq -axis currents can be well suppressed simply by the conventional PI controller and dedicated feed-forward compensation. It also shows that the decoupling fault-tolerant control based on the proposed modelling and control method has excellent dynamic performance, which is equivalent to the vector space decomposition control for the healthy machine.

1 | INTRODUCTION

Reliability has always been a major concern in many electrical drive applications such as automotive, aircraft, wind power and transportation [1–5]. Usually, the fault-tolerant drive system consists of a specifically designed electrical machine [5] and a fault-tolerant inverter topology plus a suitable remedy strategy that can drive the system in the postfault operation [6].

In the previous study, the fault-tolerant control has been investigated extensively for single three-phase machines. The analysis presented in [7] leads to an important conclusion that it is still possible to apply a rotating magnetomotive force (MMF) to the machine by changing the phase currents of the remaining phases with a new amplitude and phase offset angle under open-phase fault.

Early in the 1990s, the modelling and field-oriented control of a single three-phase induction machine (IM) under open-phase fault is presented in [8]. A unified modelling and control approach for a three-phase IM drive with a structural unbalance (one phase open) is developed, which is also used to perform field orientation by exploiting a suitable reference frame transformation [9]. The vector control for a single three-phase permanent magnet synchronous machine (PMSM) under open-phase fault is introduced in [1, 9]. As one phase is open, the system becomes unbalanced. A new single three-phase PMSM mathematical model is introduced to provide an effective solution to implement field-oriented control under open-phase fault. Meanwhile, additional power devices and the availability of the neutral point of the stator windings [10–12] or open-end winding configuration [13] are required for the

regulation of the currents in the other two phases independently.

Recently, several reconfigurable fault-tolerant multiphase PMSM drive systems have been developed, such as the conventional voltage source inverter (VSI), reduced switch-count converter, dual supply inverters, and multilevel inverters [14, 15], e.g. the postfault full torque-speed of dual three-phase interior-type PMSM (IPMSM) with the configuration of the neutral points to either isolated or connected is explored in [16]. A five-leg converter with a shared leg connected to two phase windings [17] could be used when one phase of dual three-phase PMSM (DT-PMSM) drive is open. However, extra hardware, such as the triodes for alternating current or some power switches is required, increases the system cost. Therefore, it is of academic and industrial value to investigate the fault-tolerant control of multiphase PMSM based on the conventional drive without any topology reconfiguration.

Based on the conventional multiphase drive, a synchronous-frame current controller of a five-phase IPMSM with open phases is proposed in [18], which enables the current to be regulated without a steady-state error. Although the authors claim that the basic concepts can be extended to the n -phases machine with multiple open phases, no indication is given to the configurations that are different from five-phase machines, especially to the asymmetrical DT-PMSM with a shifted angle of 30° between the two sets of three-phase windings. Meanwhile, it does not provide any evaluation of the dynamic performance of the faulty drive system. A decoupled mathematical model of the five-phase PMSM under single-phase open-circuit fault is derived and a feed-forward compensation is proposed to eliminate the influences of certain factors and decrease the current ripple [19]. However, as the surface-mounted PMSM is investigated in [19], the second harmonic inductances in the self-inductance and mutual-inductance are not considered in the modelling. There are second harmonic inductances in the inset mounted PMSM or in the surface-mounted PMSM if it is saturated.

The mathematical modelling and control of the six-phase symmetrical (shift 60° between two sets of three-phase windings) IM with up to three open phases are presented in [20], where the six-phase IM has only one neutral point. A general decoupled model of the IM with open phases and a new control method of current reconfiguration is proposed to reduce the pulsating torque and the machine losses. In [21], a simple feed-forward voltage compensation in the harmonic subplane is proposed to reduce the torque oscillations in the six-phase IM due to the open phase fault. However, there are no second harmonic inductances and permanent magnet (PM) flux-linkages in the faulty six-phase IM. When the six-phase or DT-PMSM is faulty with one phase open, there might be second harmonic inductance in the self-inductance and mutual inductance between phases. Besides, the permanent flux-linkage is also unbalanced, therefore, the mathematical modelling of DT-PMSM and corresponding control methodology will be different from [21].

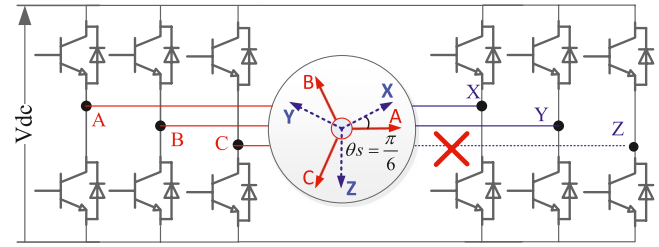


FIGURE 1 Dual three-phase drive system with phase Z open

In terms of DT-PMSM with two isolated neutral points for each set of three-phase windings, Figure 1, a non-sinusoidal current, including the second-order harmonics in the synchronous rotating reference frame, that is, dq -frame, is proposed to reduce the torque ripple of a dual three-phase PM machine under one-phase open circuit failure conditions [22]. In [23], a genetic algorithm is applied to optimise the stator currents to maximise the average torque and minimise the torque ripple under open-phase fault in the DT-PMSM with a shift angle of 30° . However, neither of the aforementioned methods introduces the modelling of the faulty machine.

In [24], different cases of open-circuited faulty phases are analysed and their fault-tolerant controllability in the general case is investigated for six-phase PM bearing-less machines, including the feasibility of fault-tolerant control with single, double, or triple faulty phases. However, this drive system is based on the open-winding configuration [13] and the current in each phase can be controlled individually. Meanwhile, the mathematical modelling of the six-phase machine is not introduced.

A fault-tolerant control is proposed for DT-PMSM drives with different phase shift angles between the two sets of three-phase windings under open-phase faults [25], where the torque capability and power loss are compared among four operation modes, that is, normal model, single three-phase mode, minimum copper loss control, and maximum torque control. The fault-tolerant control [25] focuses on the maximisation of the torque capacity with consideration of the overcurrent protection and reconfiguration of postfault operation currents rather than the mathematical modelling and decoupling vector control methodology. Meanwhile, two same surface-mounted three-phase traction PMSMs are coupled together to simulate the DT-PMSM, and therefore, the mutual coupling between two sets of single three-phase windings is not considered in [25].

The mathematical model of the DT-PMSM with one open phase (Figure 1) is introduced by the vector space decomposition modelling method in [26]. However, the inductance modelling is simplified and the second harmonic inductance [27] is not considered in [26]. Therefore, the mathematical modelling of the DT-PMSM with one phase open is not precise and accurate. Meanwhile, there are second harmonics in the PM flux-linkage in the dq -frame [26], and therefore, it cannot suppress the second harmonic currents by the conventional PI controller. Although the second harmonic

currents can be suppressed by the PI plus resonant control or dual PI controller [28, 29], they suffer from stability issues and slow dynamical performance at slow speed or standstill in the electrical drive application.

A generic and precise mathematical modelling and decoupling vector control for DT-PMSM (asymmetrical, shift angle 30°) with one phase open is proposed based on Figure 1, accounting for the mutual coupling between two sets of three-phase windings and the second harmonic inductance in the self-inductance and mutual inductances between phases. Inspired by the reference frame transformations introduced in [1] to obtain a decoupling dq -frame model for the faulty single three-phase PMSM similar to that normally used for machines working in healthy conditions, the fault-tolerant vector control of DT-PMSM is introduced here, with both the asymmetric PM flux-linkages and currents in dq -frame in the conventional vector controlling the turn into DC value in the dq -frame, and therefore, the conventional PI controller could be used to regulate the currents. Based on the proposed mathematical modelling, a decoupling fault-tolerant vector control scheme with/without the feed-forward control is used for its validation.

2 | MATHEMATICAL MODELLING OF DUAL THREE-PHASE PMSM WITH ONE PHASE OPEN

The variable speed drive (VSD) theory is introduced in [30, 31] for the healthy dual three-phase machine. The six-dimensional machine system can be decomposed into three orthogonal subspaces, that is, $\alpha\beta$, z_1z_2 , o_1o_2 subplanes. By the transformation matrix, different harmonics are mapped to different subplanes. The fundamental and $(12k \pm 1)$ th, $k = 1, 2, \dots$ harmonics in the real frame are mapped to $\alpha\beta$ subplane; the $(6k \pm 1)$ th, $k = 1, 3, 5, \dots$ harmonics in the real frame are mapped to z_1z_2 subplane; the $(3k)$ th, $k = 0, 1, 3, 5, \dots$ harmonics in the real frame are mapped to o_1o_2 subplane. However, the full-order matrix transformation no longer functions properly when one phase is open, where there is a conflict of interest between current controllers in $\alpha\beta$ and z_1z_2 subplanes [32]. Using the same concept of the VSD theory, the modelling and vector control of the six-phase asymmetric IM with one phase open are presented in [33, 34], an unbalanced stationary to synchronous rotating reference frame transformation for stator currents are developed. Consequently, the existing field-oriented control becomes applicable in the postfault operation.

Considering the DT-PMSM, without loss of generality, the phase Z is assumed to be the open phase in this case study, by matrix transformation shown in Equation (1), the variables in the abc - xyz frame, Figure 1 can be converted into two decoupled subplanes: $\alpha\beta$ subplane and z subplane, which are orthogonal to each other. All the electromechanical energy conversion-related variable components are mapped to the $\alpha\beta$ subplane, and all the nonelectromechanical energy conversion-related variable components are projected to the z subplane.

$$\begin{aligned} & [F_\alpha \ F_\beta \ F_{z1} \ F_{z2} \ F_{z3}]^T \\ & = [T_5] \cdot [F_a \ F_x \ F_b \ F_y \ F_c]^T \end{aligned} \quad (1)$$

where $[T_5]$ can be expressed as Equation (2) if phase Z is open and θ_s is equal to $\pi/6$.

$$\begin{aligned} & [T_5] \\ & = \frac{1}{3} \begin{bmatrix} \cos(0\theta_s) & \cos(1\theta_s) & \cos(4\theta_s) & \cos(5\theta_s) & \cos(8\theta_s) \\ \sin(0\theta_s) & 0 & \sin(4\theta_s) & 0 & \sin(8\theta_s) \\ \cos(0\theta_s) & \cos(5\theta_s) & \cos(8\theta_s) & \cos(1\theta_s) & \cos(4\theta_s) \\ 1 & 0 & 1 & 0 & 1 \\ 0 & 1 & 0 & 1 & 0 \end{bmatrix}. \end{aligned} \quad (2)$$

where F can be R , v , i , ψ_s or ψ_f , which correspond to stator resistance, voltage, current, stator flux-linkage or PM flux-linkage, respectively.

2.1 | Mathematical modelling in abc - xyz frame

The voltage and flux-linkage equations for DT-PMSM with phase Z open in the abc - xyz frame can be expressed as:

$$[v_s] = [R_s][i_s] + \frac{d}{dt}[\psi_s] \quad (3)$$

$$[\psi_s] = [L_s][i_s] + [\psi_f] \quad (4)$$

where $[R_s]$, $[v_s]$, $[i_s]$, $[\psi_s]$ and $[\psi_f]$ correspond to stator resistance, voltage, current, stator flux-linkage and PM flux-linkage with one phase open in abc - xyz frame, respectively. $[L_s]$ is the inductance matrix [27] for dual three-phase PM machine with phase Z open, which can be expressed as Equation (5)

$$[L_s] = \begin{bmatrix} L_{aa} & M_{ax} & M_{ab} & M_{ay} & M_{ac} \\ M_{xa} & L_{xx} & M_{xb} & M_{xy} & M_{xc} \\ M_{ba} & M_{bx} & L_{bb} & M_{by} & M_{bc} \\ M_{ya} & M_{yx} & M_{yb} & L_{yy} & M_{yc} \\ M_{ca} & M_{cx} & M_{cb} & M_{cy} & L_{cc} \end{bmatrix} \quad (5)$$

Assuming the induced back electromotive force (EMF) is sinusoidal; eddy current and hysteresis losses, mutual leakage inductance, saturation are neglected; the inductance of higher order than the second-order and mutual leakage inductance [27, 35, 36] is not considered, the self-inductance of the phases can be expressed as:

$$L_{pp} = L_{sl} + L_{dqavg} + L_{dqdiff} \cos(2\theta_p) \quad (6)$$

$$L_{dqavg} = (L_d + L_q)/2 \quad (7)$$

$$L_{dqdiff} = (L_d - L_q)/2 \quad (8)$$

The mutual inductance between phases in each set of three-phase windings can be expressed as:

$$M_{PQ} = M_{dqavg} \cos(\theta_P - \theta_Q) + M_{dqdiff} \cos(\theta_P + \theta_Q) \quad (9)$$

The mutual inductance between phases in a different set of three-phase windings can be expressed as:

$$M_{PQ} = M_{dq12avg} \cos(\theta_P - \theta_Q) + M_{dq12diff} \cos(\theta_P + \theta_Q) \quad (10)$$

where P stands for phase a , x , b , y , c or z , while Q represents another phase that is different with phase P . θ_P and θ_Q are the electrical angles of the axis of phase P and phase Q 's winding shifted from d -axis of PM rotor. L_{sl} is the phase leakage inductance, $(L_{sl} + L_d)$ is the phase self-inductance when the axis of phase winding is aligned to d -axis, $(L_{sl} + L_q)$ is the phase self-inductance when the axis of phase winding is aligned to the q -axis. $M_{dqavg} \cos(\theta_P - \theta_Q)$ and $M_{dqdiff} \cos(\theta_P - \theta_Q)$ are average and second harmonic mutual inductances between phases in each set of three-phase windings, respectively. $M_{dq12avg} \cos(\theta_P - \theta_Q)$ and $M_{dq12diff} \cos(\theta_P - \theta_Q)$ are average and second harmonic mutual inductances between phases in a different set of three-phase windings, respectively.

2.2 | Mathematical modelling in $\alpha\beta$ - $z_1z_2z_3$ subplanes

Applying Equation (1) to Equations (3) and (4) respectively, the voltage and flux-linkage equations in $\alpha\beta$ - $z_1z_2z_3$ subplanes can be expressed as Equations (11) and (12) respectively.

$$[v_{\alpha\beta z}] = [R_{\alpha\beta z}][i_{\alpha\beta z}] + \frac{d}{dt}[\psi_{s\alpha\beta z}] \quad (11)$$

$$[\psi_{s\alpha\beta z}] = [L_{\alpha\beta z}][i_{\alpha\beta z}] + [\psi_{f\alpha\beta z}] \quad (12)$$

where $[v_{\alpha\beta z}]$ is equal to $[T_5][v_s]$; $[i_{\alpha\beta z}]$ is equal to $[T_5][i_s]$; $[\psi_{s\alpha\beta z}]$ is equal to $[T_5][\psi_s]$; $[\psi_{f\alpha\beta z}]$ is equal to $[T_5][\psi_f]$; $[L_{\alpha\beta z}]$ is equal to $[T_5][L_s][T_5]^{-1}$ and $[R_{\alpha\beta z}]$ is equal to $[T_5][R_s][T_5]^{-1}$.

As i_{z2} and i_{z3} are zero in the dual three-phase system with two isolated neutral points when phase Z is open, only the flux-linkages in the $\alpha\beta$ subplane and z_1 -axis need to be considered. The stator flux-linkage in $\alpha\beta$ subplane $[\psi_{s\alpha\beta}]$ can be separated from Equation (12) and expressed as Equation (13).

$$[\psi_{s\alpha\beta}] = [L_{\alpha\beta}][i_{\alpha\beta}] + [M_{\alpha\beta z_1}]i_{z_1} + [\psi_{f\alpha\beta}] \quad (13)$$

where $[L_{\alpha\beta}]$ and $[M_{\alpha\beta z_1}]$ are shown in Equations (A2) and (A8), respectively, $[\psi_{s\alpha\beta}] = [\psi_{s\alpha}\psi_{s\beta}]^T$, $[i_{\alpha\beta}] = [i_{\alpha}i_{\beta}]^T$.

The stator flux-linkage ψ_{sz1} in z_1 -axis can also be separated from Equation (12) and expressed as Equation (14).

$$\psi_{sz1} = L_{z1}i_{z1} + M_{z1\beta}i_{\beta} + \psi_{fz1} \quad (14)$$

where L_{z1} and $M_{z1\beta}$ are shown in Equations (A9) and (A10), respectively.

It can be seen from Equations (13) and (14) that there is a mutual coupling between the $\alpha\beta$ subplane and the $z_1z_2z_3$ subplane, the mathematical model is not fully decomposed if $M_{z1\beta}$ and $[M_{\alpha\beta z_1}]$ are not zero.

The voltage equations in the $\alpha\beta$ subplane and $z_1z_2z_3$ subplane can be separated from Equation (11) and expressed as Equations (15) and (16), respectively, if each phase winding resistance is R .

$$[v_{\alpha\beta}] = R[i_{\alpha\beta}] + \frac{d}{dt}[\psi_{s\alpha\beta}] \quad (15)$$

$$v_{z1} = Ri_{z1} + \frac{d}{dt}\psi_{sz1} \quad (16)$$

The PM flux-linkage of each phase is proportional to the phase back-EMF, if only the fundamental component is considered, and the PM flux-linkage of each phase can be expressed as:

$$\begin{bmatrix} \psi_{fa} \\ \psi_{fx} \\ \psi_{fb} \\ \psi_{fy} \\ \psi_{fc} \end{bmatrix} = \psi_m \begin{bmatrix} \cos(\theta - 0\theta_s) \\ \cos(\theta - 1\theta_s) \\ \cos(\theta - 4\theta_s) \\ \cos(\theta - 5\theta_s) \\ \cos(\theta - 8\theta_s) \end{bmatrix} \quad (17)$$

where the subscript 'f' indicates the PM flux-linkage, ψ_m is its amplitude and θ is the electrical angle of PM rotor, then the PM flux-linkage in $\alpha\beta$ - $z_1z_2z_3$ subplanes can be expressed as:

$$\begin{bmatrix} \psi_{f\alpha} \\ \psi_{f\beta} \\ \psi_{fz1} \\ \psi_{fz2} \\ \psi_{fz3} \end{bmatrix} = [T_5] \begin{bmatrix} \psi_{fa} \\ \psi_{fx} \\ \psi_{fb} \\ \psi_{fy} \\ \psi_{fc} \end{bmatrix} = \psi_m \begin{bmatrix} \cos(\theta) \\ 1/2 \cdot \sin(\theta) \\ 0 \\ 0 \\ 1/3 \cdot \sin(\theta) \end{bmatrix} \quad (18)$$

Equation (18) indicates that the PM flux-linkage in the $\alpha\beta$ subplane is not balanced. To obtain a balanced PM flux-linkage in the $\alpha\beta$ subplane, an additional matrix transformation is required. Similar to the method introduced in the modelling of single three-phase PMSM with one phase open [1], the additional matrix $[B]$ can be expressed as:

$$[B] = \begin{bmatrix} 1 & 0 \\ 0 & 2 \end{bmatrix} \quad (19)$$

The transformation can be expressed as:

$$[F_{\alpha 2\beta 2}] = \begin{bmatrix} F_{\alpha 2} \\ F_{\beta 2} \end{bmatrix} = [B] \begin{bmatrix} F_{\alpha} \\ F_{\beta} \end{bmatrix} \quad (20)$$

Substituting PM flux-linkages in $\alpha\beta$ subplane into Equation (20), the PM flux-linkages are mapped to a new stationary frame, that is, the $\alpha_2\beta_2$ -frame, which can be expressed as:

$$\begin{bmatrix} \psi_{f\alpha 2} \\ \psi_{f\beta 2} \end{bmatrix} = [B] \begin{bmatrix} \psi_{f\alpha} \\ \psi_{f\beta} \end{bmatrix} = \psi_m \begin{bmatrix} \cos(\theta) \\ \sin(\theta) \end{bmatrix} \quad (21)$$

Equation (21) shows that the PM flux-linkages in $\alpha_2\beta_2$ -frame are balanced. By applying Equation (20) to Equation (13), the voltage equation in $\alpha_2\beta_2$ -frame can be expressed as:

$$[v_{\alpha 2} \ v_{\beta 2}]^T = R[i_{\alpha 2} \ i_{\beta 2}]^T + \frac{d}{dt}[\psi_{s\alpha 2} \ \psi_{s\beta 2}]^T \quad (22)$$

The stator flux-linkage in $\alpha_2\beta_2$ -frame can be expressed as:

$$\begin{bmatrix} \psi_{s\alpha 2} \\ \psi_{s\beta 2} \end{bmatrix} = [L_{\alpha 2\beta 2}] \begin{bmatrix} i_{\alpha 2} \\ i_{\beta 2} \end{bmatrix} + [M_{\alpha 2\beta 2z1}]i_{z1} + \begin{bmatrix} \psi_{f\alpha 2} \\ \psi_{f\beta 2} \end{bmatrix} \quad (23)$$

where $[L_{\alpha 2\beta 2}]$ and $[M_{\alpha 2\beta 2z1}]$ are shown in Equations (A11) and (A12), respectively.

2.3 | Mathematical modelling in dq -frame

On applying the rotation transformation for the voltages and flux-linkages in the $\alpha_2\beta_2$ -frame, the dq -axis voltages and flux-linkages can be expressed as:

$$[v_d \ v_q]^T = [T_{dq}] [v_{\alpha 2} \ v_{\beta 2}]^T \quad (24)$$

$$[\psi_{sd} \ \psi_{sq}]^T = [T_{dq}] [\psi_{s\alpha 2} \ \psi_{s\beta 2}]^T \quad (25)$$

$$[\psi_{fd} \ \psi_{fq}]^T = [T_{dq}] [\psi_{f\alpha 2} \ \psi_{f\beta 2}]^T \quad (26)$$

where $[T_{dq}]$ is the rotation transformation matrix, shown as:

$$[T_{dq}] = \begin{bmatrix} \cos(\theta) & \sin(\theta) \\ -\sin(\theta) & \cos(\theta) \end{bmatrix} \quad (27)$$

Substitute Equation (21) into Equation (26), the dq -axis PM flux-linkages can be expressed as:

$$[\psi_{fdq}] = [\psi_{fd} \ \psi_{fq}]^T = [\psi_m \ 0]^T \quad (28)$$

As the expected trajectory of current vector $\mathbf{i}_{\alpha\beta} = i_{\alpha} + ji_{\beta}$ is a circle for a rotating circle-based MMF in the machine with constant speed, after transformation to $\alpha_2\beta_2$ -frame, the trajectory of current vector $\mathbf{i}_{\alpha 2\beta 2} = i_{\alpha 2} + ji_{\beta 2}$ is not a circle anymore. Therefore, if $[T_{dq}]$ is applied to $[i_{\alpha 2\beta 2}]$ directly, i_d and i_q will not be a DC value. Consequently, it is not easy to maintain the steady-state errors to zero in dq -frame as the dq -axis currents are AC values. To solve this issue, a new matrix conversion Equation (29) is introduced. By applying Equation (29) to currents in $\alpha_2\beta_2$ -frame, the currents in dq -frame can be expressed as:

$$[i_d \ i_q]^T = [T_{dq-I}] [i_{\alpha 2} \ i_{\beta 2}]^T \quad (29)$$

where

$$[T_{dq-I}] = \begin{bmatrix} \cos(\theta) & \sin(\theta)/2 \\ -\sin(\theta)/2 & \cos(\theta) \end{bmatrix} \quad (30)$$

Then, Equation (29) can also be rewritten as:

$$\begin{bmatrix} i_d \\ i_q \end{bmatrix} = [T_{dq-I}] \begin{bmatrix} i_{\alpha 2} \\ i_{\beta 2} \end{bmatrix} = [T_{dq-I}] [B] \begin{bmatrix} i_{\alpha} \\ i_{\beta} \end{bmatrix} = [T_{dq}] \begin{bmatrix} i_{\alpha} \\ i_{\beta} \end{bmatrix} \quad (31)$$

The stator flux-linkages in dq frame can be expressed as:

$$\begin{aligned} \begin{bmatrix} \psi_{sd} \\ \psi_{sq} \end{bmatrix} &= [T_{dq}] \left([L_{\alpha 2\beta 2}] \begin{bmatrix} i_{\alpha 2} \\ i_{\beta 2} \end{bmatrix} + [M_{\alpha 2\beta 2z1}]i_{z1} + \begin{bmatrix} \psi_{f\alpha 2} \\ \psi_{f\beta 2} \end{bmatrix} \right) \\ &= \left([T_{dq}] [L_{\alpha 2\beta 2}] [T_{dq-I}]^{-1} \right) \left([T_{dq-I}] \begin{bmatrix} i_{\alpha 2} \\ i_{\beta 2} \end{bmatrix} \right) \\ &\quad + [T_{dq}] [M_{\alpha 2\beta 2z1}]i_{z1} + [T_{dq}] \begin{bmatrix} \psi_{f\alpha 2} \\ \psi_{f\beta 2} \end{bmatrix} \end{aligned} \quad (32)$$

Define

$$[L_{dq}] = [T_{dq}] [L_{\alpha 2\beta 2}] [T_{dq-I}]^{-1} \quad (33)$$

$$[M_{dqz1}] = [T_{dq}] [M_{\alpha 2\beta 2z1}] \quad (34)$$

then Equation (32) can be rewritten as:

$$\begin{bmatrix} \psi_{sd} \\ \psi_{sq} \end{bmatrix} = [L_{dq}] \begin{bmatrix} i_d \\ i_q \end{bmatrix} + [M_{dqz1}]i_{z1} + \begin{bmatrix} \psi_{fd} \\ \psi_{fq} \end{bmatrix} \quad (35)$$

where $[L_{dq}]$ and $[M_{dqz1}]$ can be expressed in Equations (A22) and (A27).

Apply Equation (27) to Equation (22), i.e.,

$$\begin{aligned} [T_{dq}] \begin{bmatrix} v_{\alpha 2} \\ v_{\beta 2} \end{bmatrix} &= [T_{dq}] R [T_{dq-I}]^{-1} \left([T_{dq-I}] \begin{bmatrix} i_{\alpha 2} \\ i_{\beta 2} \end{bmatrix} \right) \\ &+ [T_{dq}] \frac{d}{dt} \left([T_{dq}]^{-1} \left([T_{dq}] \begin{bmatrix} \psi_{\alpha 2} \\ \psi_{\beta 2} \end{bmatrix} \right) \right) \end{aligned} \quad (36)$$

Then Equation (36) can be simplified as:

$$\begin{bmatrix} v_d \\ v_q \end{bmatrix} = [R_{dq}] \begin{bmatrix} i_d \\ i_q \end{bmatrix} + \frac{d}{dt} \begin{bmatrix} \psi_{sd} \\ \psi_{sq} \end{bmatrix} + \omega \begin{bmatrix} -\psi_{sq} \\ \psi_{sd} \end{bmatrix} \quad (37)$$

where

$$[R_{dq}] = R \begin{bmatrix} 1 & 0 \\ 0 & 1 \end{bmatrix} + \frac{1}{2} R [M(\theta)] \quad (38)$$

$$[M(\theta)] = \begin{bmatrix} 1 - \cos(2\theta) & \sin(2\theta) \\ \sin(2\theta) & 1 + \cos(2\theta) \end{bmatrix} \quad (39)$$

Neglecting the reluctance torque, the electromagnetic torque can be expressed as Equation (40), where p is the number of pole pairs. The derivation is detailed in Section 7-Appendix.

$$T_e = 3p(-i_d \psi_{fq} + i_q \psi_{fd}) \quad (40)$$

It is worth noting that the modelling is based on the conventional dual three-phase VSIs. When one phase is open, it is simply isolated from the system without any extra hardware reconfiguration. The open phase scenarios of DT-PMSM can be listed as Table 1 according to the number of the open phase it can operate with reduced capability in the scenarios of one phase open, two phases open and three phases open (phase ABC or phase XYZ open only). Although the mathematical modelling is focused on the scenario of one phase open, the methodology can be extended to the scenarios of two phases open and three-phase open.

3 | FAULT-TOLERANT VECTOR CONTROL SCHEME

The fault-tolerant vector control of DT-PMSM with one phase open illustrated in Figure 2 is used to verify the correctness of the proposed mathematical modelling. Within and current limit for power converters operating normally and under postfault operation conditions, to achieve the same torque, the peak current of DT-PMSM with two isolated neutral points will be 1.732, 1.803 or 2 times of peak current in the healthy mode if the maximum torque control, minimum copper loss control or

TABLE 1 Open phase scenarios of dual three-phase PMSM

Categories	Scenarios					
One phase	A	B	C	X	Y	Z
Two phases	AB	BC	CA	XY	YZ	ZX
	AX	AY	AZ	BX	BY	BZ
	CX	CY	CZ			
Three phases (can work)	ABC	XYZ				
Three phases (cannot work)	AXY	AYZ	AZX	BXY	BYZ	BZX
	CXY	CYZ	CZX	ABX	ABY	ABZ
	BCX	BCY	BCZ	CAX	CAY	CAZ
Four phases	Cannot work					
Five phases	Cannot work					
Six phases	Cannot work					

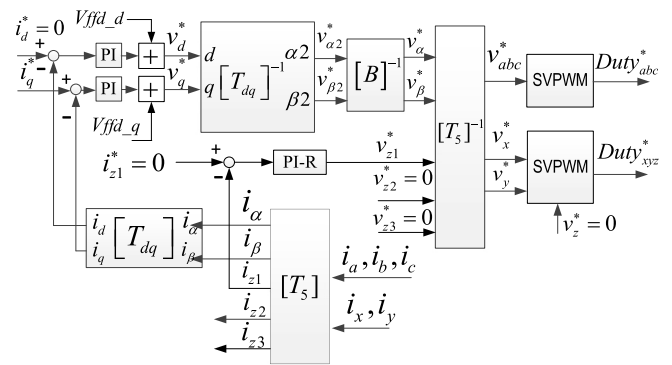
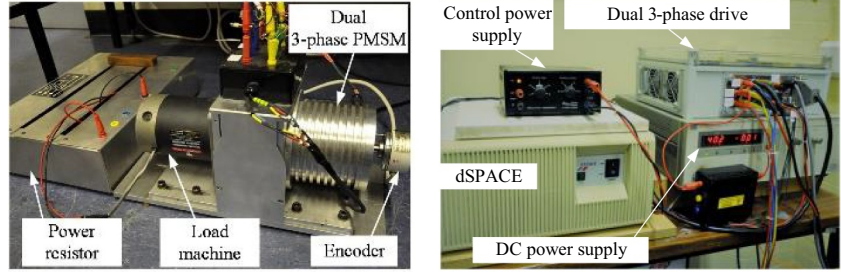


FIGURE 2 Decoupling vector control with feedforward compensation for DT-PMSM with phase-Z open

single three-phase mode control [22, 26] is used respectively. Therefore, the torque will be 1/1.732, 1/1.803 and 1/2 of the maximum torque of the healthy mode respectively. In terms of the voltage limit, the power capacity will be constrained by the DC bus voltage. As the trajectory of the output voltage vector under postfault operating conditions is not a circle anymore, and thus, it is challenging to determine the power capability, which can be obtained by an offline optimisation that takes into account simultaneously the voltage and current constraints [16]. In this case study, the minimum copper loss control [25, 37] is adopted for investigation. Two conventional PI controllers are used to regulate the dq -axis currents in the dq -frame. By inverse $[T_{dq}]$ transformation to v_d^* and v_q^* , the $v_{\alpha 2}^*$ and $v_{\beta 2}^*$ in $\alpha 2\beta 2$ -frame can be deduced, and then, these signals are converted to v_{α}^* and v_{β}^* in $\alpha\beta$ -frame by inverse $[B]$ transformation. As shown in the voltage Equation (16), there is a fundamental component in ψ_{z1} in Equation (14). Therefore, the PI plus resonance controller (PI-R) with the centre frequency of a fundamental component is used to regulate the i_{z1} current to zero for minimum copper loss control [25, 37]. The output of the PI-R controller is v_{z1}^* . When all the signals v_{α}^* ,

FIGURE 3 Experimental setups for DT-PMSM



v_{β}^* , v_{z1}^* , v_{z2}^* and v_{z3}^* are ready, the v_a^* , v_b^* , v_c^* , v_x^* and v_y^* can be obtained by inverse $[T_5]$ transformation, and then, the duties can be derived by the conventional space vector pulse width modulation (SVPWM) generation.

V_{ffd_d} and V_{ffd_q} are the feed-forward voltages in the d -axis and q -axis, respectively, which can be expressed as:

$$\begin{bmatrix} v_{ffd_d} \\ v_{ffd_q} \end{bmatrix} = \frac{1}{2}R[M(\theta)] \begin{bmatrix} i_d \\ i_q \end{bmatrix} + \omega \begin{bmatrix} -\psi_{sq} \\ \psi_{sd} \end{bmatrix} \quad (41)$$

From the second part in Equation (38), it can be seen that the resistances in the dq -frame vary with the rotor position. Besides, there are also second harmonics in $-\omega\psi_q$ and $\omega\psi_d$ as there are second harmonic inductances in $[L_{dq}]$ in Equation (A22) and $[M_{dqz1}]$ in Equation (A27). If the voltage in Equation (41) is compensated accurately by the feed-forward compensation, the current control in the faulty condition can be treated as the same as that in healthy condition.

4 | EXPERIMENTS

The test platform is constructed based on dSPACEDS1005, which is shown in Figure 3. The dual three-phase VSI power topology is the same as Figure 1, while the phase Z is left open deliberately. Two single three-phase VSIs share the same DC voltage source. Two independent SVPWM modulators are used to generate pulse width modulation (PWM) duties for each set of three-phase windings. The prototype machine is coupled to a DC generator, which is connected to an adjustable power resistor. The load can be adjusted by changing the resistance of the power resistor. If the friction is neglected, the electromagnetic torque could be reflected by the speed.

In the fault-tolerant control, the postfault operation should be in a similar way of the healthy machine with a circular trajectory for the current vector, therefore, the rotating MMF will be the same as the healthy machine when the DT-PMSM is faulty with one phase open [7]. In this experiment, the minimum copper loss control [25, 37] is adopted, where the trajectory of the current vector is the same as that of the healthy machine, whilst the copper loss is the minimum. With this control strategy, the phase currents should be the same as

Equation (42), where I_m is the amplitude of the current vector, and θ is the electrical rotor position.

$$\begin{bmatrix} i_a \\ i_x \\ i_b \\ i_y \\ i_c \end{bmatrix} = I_m \begin{bmatrix} \cos(\theta + \pi/2) \\ \sqrt{3}/2\cos(\theta + \pi/2) \\ -1/2\cos(\theta + \pi/2) + \sqrt{3}\sin(\theta + \pi/2) \\ -\sqrt{3}/2\cos(\theta + \pi/2) \\ -1/2\cos(\theta + \pi/2) - \sqrt{3}\sin(\theta + \pi/2) \end{bmatrix} \quad (42)$$

On applying Equation (1) to Equation (42), the currents in $\alpha\beta$ - $z_1z_2z_3$ subplanes are:

$$\begin{bmatrix} i_\alpha & i_\beta & i_{z1} & i_{z2} & i_{z3} \end{bmatrix}^T = I_m \begin{bmatrix} -\sin(\theta) & \cos(\theta) & 0 & 0 & 0 \end{bmatrix}^T \quad (43)$$

As can be seen from Equation (43), the currents in the $\alpha\beta$ subplane are balanced, and a rotating MMF can be achieved by the phase currents with a new amplitude and phase offset angle as Equation (42) under open-phase fault.

The parameters of prototype DT-PMSM are shown in Table 2 and the parameters in Table 3 are derived from the measured inductances by LCR meter. The inductances in the faulty condition with one phase open are shown in Table 4. When the machine speed is rated speed, the amplitude of variable impedance in Equation (A22) can be listed in Table 5. Since L_{dq-ac2} is much smaller than L_{dq-ac1} , the voltage disturbance in steady operation is mainly caused by L_{dq-ac1} in Equation (A22) and variable resistances in Equation (38).

The current loop is executed for every PWM cycle at 100 μ s. The overall time delay T_d including the PWM output delay, current sampling delay and processing delay, is approximately 1.5 times of PWM period, which is $T_d = 150 \mu$ s. The design principle of PI gains is that the dominant pole of $1/(Ls+R)$ is

TABLE 2 Parameters of prototype DT-PMSM

Parameters	Value	Parameters	Value
Resistance (Ω)	1.096	Power (W)	240
Flux-linkage (Wb)	0.075	Rated speed (rpm)	400
Pole pairs	5	DC link voltage (V)	40

TABLE 3 Inductances of prototype DT-PMSM

Parameters	Value (mH)	Parameters	Value (mH)
L_{sl}	0.8	L_{dqdiff}	-1.000
L_d	1.917	M_{dqavg}	-0.617
L_q	3.917	M_{dqdiff}	0.592
M_d	-0.025	$M_{dq12avg}$	0.984
M_q	-1.209	$M_{dq12diff}$	-0.265
L_{dqavg}	2.917		

TABLE 4 Inductances in the faulty condition with one phase open

Parameters	Value (mH)	Parameters	Value (mH)
L_d^{equ}	4.58	L_{dq_ac1}	1.932
L_q^{equ}	5.19	L_{dq_ac2}	0.49
		M_{dqz1_ac}	0.49

TABLE 5 Amplitude of variable impedance with rated speed

Parameters	Value (Ω)
The second part in Equation (A22): $\omega L_{dq_ac1}/2$	0.202
The third part of Equation (A22) $\omega L_{dq_ac2}/2$	0.051
The variable resistor in Equation (38): $R/2$	0.548

cancelled by the zero-point of the PI controller [38], Then, K_p and K_i can be optimally designed as:

$$k_p = \frac{L}{4\xi^2 T_d}; k_i = \frac{R}{4\xi^2 T_d} \quad (44)$$

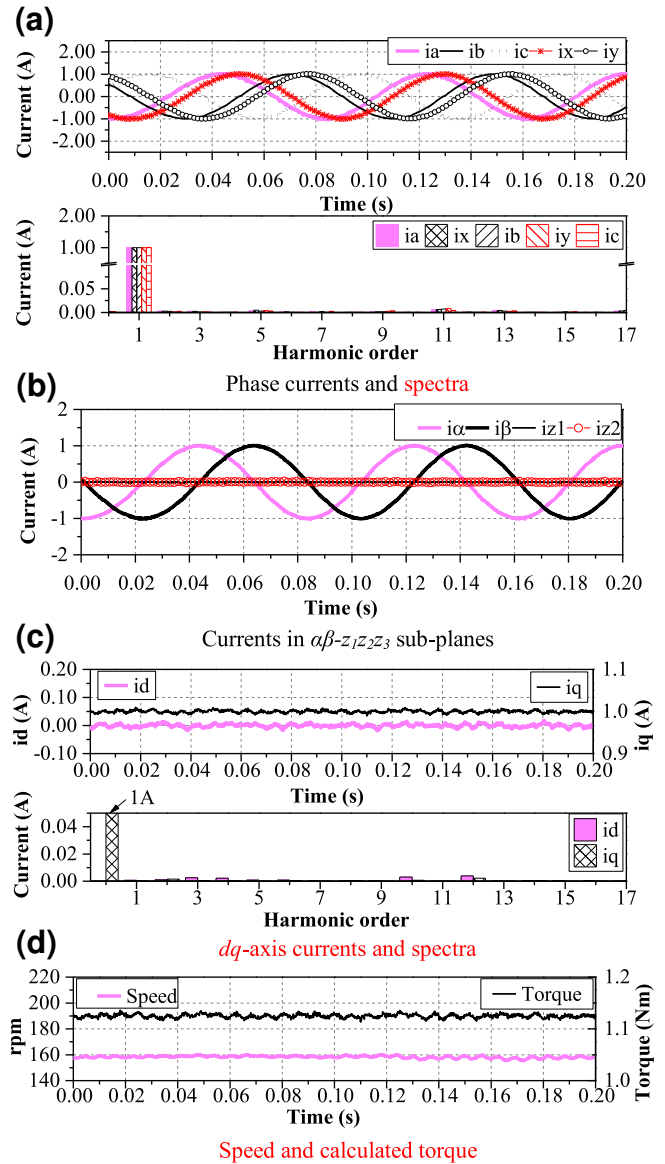
where ξ is the damping factor. In this case study, the resistance and inductances in the dq -frame vary with rotor position. As the voltage drop from $1/R * [M(\theta)]$ is compensated by feed-forward compensation, the resistance for the design of PI gains can be treated as a DC value. In terms of inductances, for simplicity, the inductance L for the calculation of K_p in Equation (44) is chosen as the minimum value in Equations (A22) and (A9), that is $L = 4.579$ mH for d -axis current regulator, $L = 5.190$ mH for the q -axis current regulator, and $L = 1.443$ mH for z_1 -axis current regulator. Besides, the cut-frequency of the practical resonant controller in z_1 -axis current regulator is chosen as 1/200 times of the resonant frequency, and its integral gain is set to be the same as the integral gain of the PI controller. Therefore, the gains of the current regulator can be listed in Table 6.

4.1 | VSD control in healthy mode

To set up the benchmark for the fault-tolerant control with one phase open, the results of VSD control in the healthy mode [31]

TABLE 6 Parameters of regulators

Parameters	Value
Proportional gain of d -axis current regulator	15.27
Integral gain of d -axis current regulator	3654
Proportional gain of q -axis current regulator	17.31
Integral gain of q -axis current regulator	3654
Proportional gain in z_1 -axis current regulator	4.81
Integral gain of in z_1 -axis current regulator	3654
Integral gain of the resonant controller in z_1 -axis	3654

**FIGURE 4** VSD control in healthy mode @ $i_q^* = 1A$

are introduced at first. The PI plus resonant control for the sixth-order harmonic in the dq -frame is used to eliminate the fifth and seventh harmonics in phase currents in the harmonic subplane

[31]. In this test, i_q^* is assigned to 1A and the experimental results are shown in Figure 4. As can be seen from Figure 4(a), the currents of phase-ABC and phase-XYZ have the same amplitude and balanced. Phase X current lags phase A current by 30°, phase Y current lags phase B current by 30°. Figure 4(b) shows that i_α and i_β in the $\alpha\beta$ subplane are very sinusoidal, i_{z1} , and i_{z2} in the z_1z_2 sub-plane are well regulated to zero. The harmonic analysis of i_d and i_q shown in Figure 4(c) indicates that there are negligible second harmonic components. The speed and calculated torque are shown in Figure 4(d). The speed is about 160rpm and the average torque is approximately 1.125Nm.

4.2 | Steady-state operation

The experiments without/with feed-forward compensation with $i_q^* = 1A$ are shown in Figures 5 and 6, respectively. From Figures 5(a) and 6(a), it can be seen that the phase currents of the first set are unbalanced, the phase current of the remaining

two phases in the second set is opposite to each other due to phase Z is open. Meanwhile, the phase current harmonic analyses in the **bottom** part of Figures 5(a) and 6(a) indicate that the phase currents are not sinusoidal, and the majority of harmonics are the third, fifth and seventh harmonics, which resulted from the asymmetric inverter nonlinearity [17]. i_α and i_β in the $\alpha\beta$ subplane shown in Figures 5(b) and 6(b) are very sinusoidal, whilst i_{z1} in Figures 5(b) and 6(b) is zero, which indicates that the minimum copper loss control is used.

There are distinct second-order current harmonics in the dq -axis current i_d and i_q in Figure 5(c) without feed-forward compensation. In contrast, with feed-forward compensation, the second harmonic currents in dq -axis current i_d and i_q , Figure 6(c), are suppressed effectively with only conventional PI control, which shows the superiority of second-order harmonic currents suppression due to the feed-forward compensation. It is

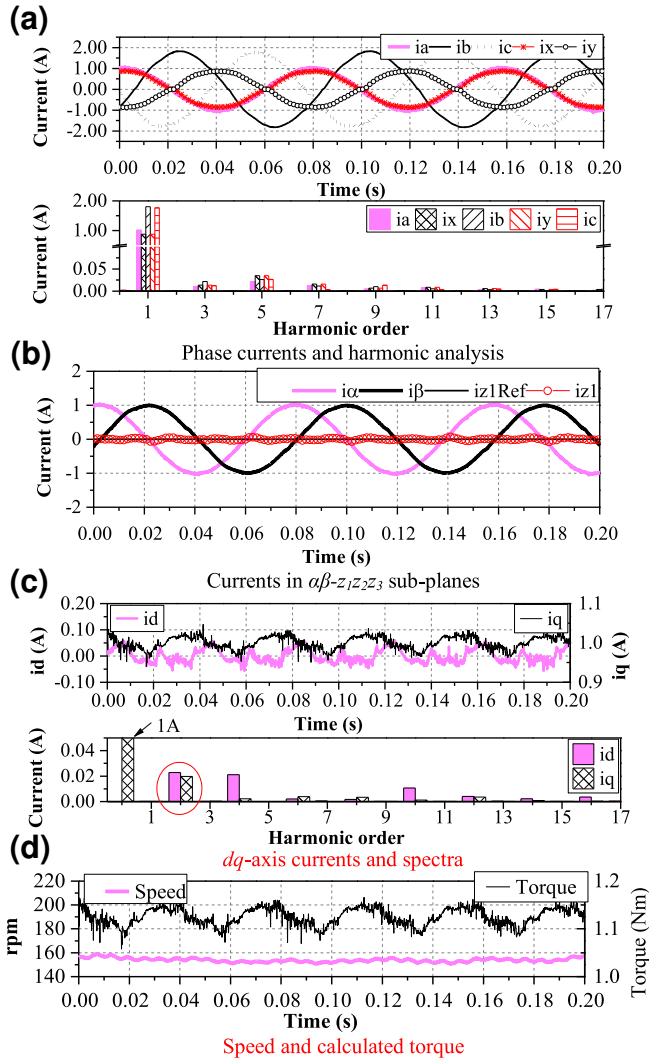


FIGURE 5 Measured results without feed-forward compensation@ $i_q^* = 1A$

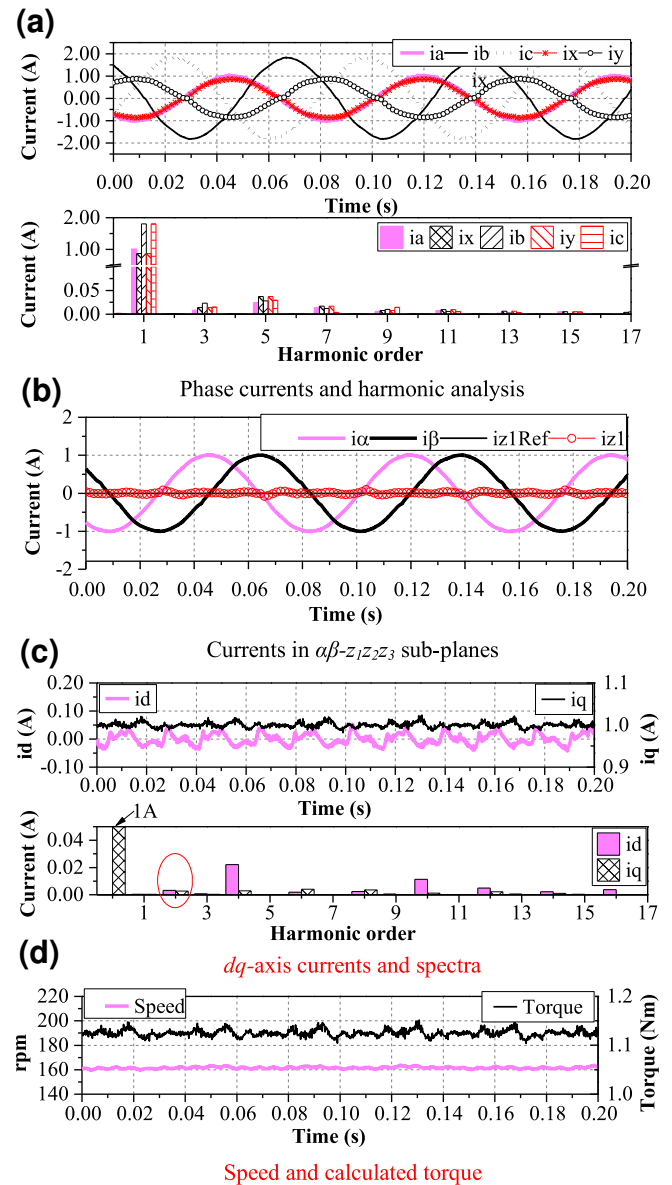


FIGURE 6 Measured results with feed-forward compensation $i_q^* = 1A$

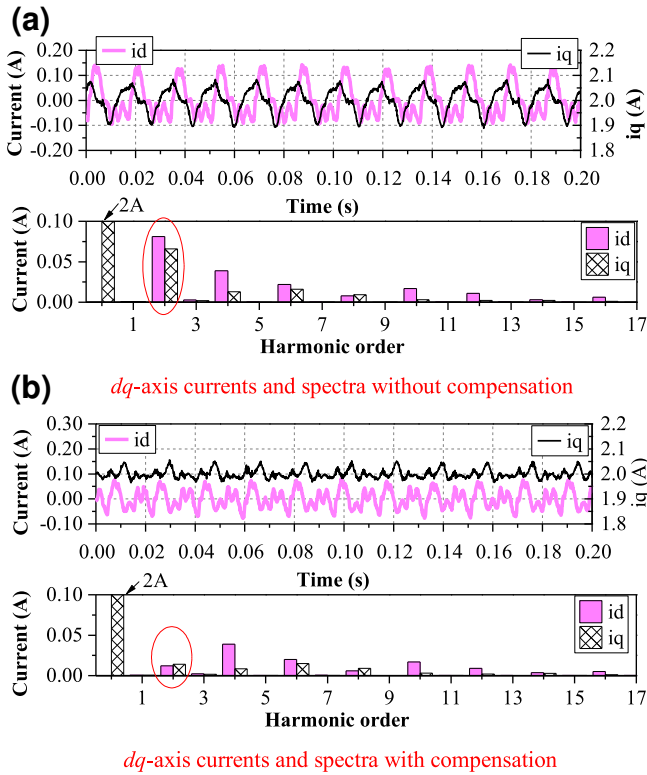


FIGURE 7 Measured results with/without feed-forward compensation @ $i_q^* = 2A$

worth noting that there is a little portion of fourth harmonic that exists in the d -axis currents in Figures 5(c) and 6(c), which is due to the voltage distortion resulting from the asymmetrical inverter nonlinearity when one phase is open [17]. The speeds and calculated torque without and with feed-forward compensation are shown in Figures 5(d) and 6(d), respectively. The speeds are both around 160rpm and very stable without obvious fluctuations. However, the calculated torque in Figure 6(d) has less oscillation than that in Figure 5(d).

To further illustrate the reasonability of the proposed mathematical modelling, the experimental results with/without feed-forward compensation under $i_q^* = 2A$ are evaluated. The profile of the phase currents and currents in $\alpha\beta$ - $z_1z_2z_3$ sub-planes are similar to the currents in Figures 5 and 6, except that the amplitudes of currents are different and the speeds are about 320rpm. Therefore, they will not be demonstrated anymore to avoid redundancy. Instead, the dq -axis currents and corresponding fast Fourier transform analysis are shown in Figure 7. The second-order harmonic is apparent in i_d and i_q (Figure 7(a)) without feed-forward compensation. With feed-forward compensation, the second-order harmonic in i_d and i_q (Fig. 7(b)) is suppressed effectively.

4.3 | Step response

In this experiment, the i_q^* reference current is stepped from 0.5 to 1 A at the time of 0.00 s. The step responses without and

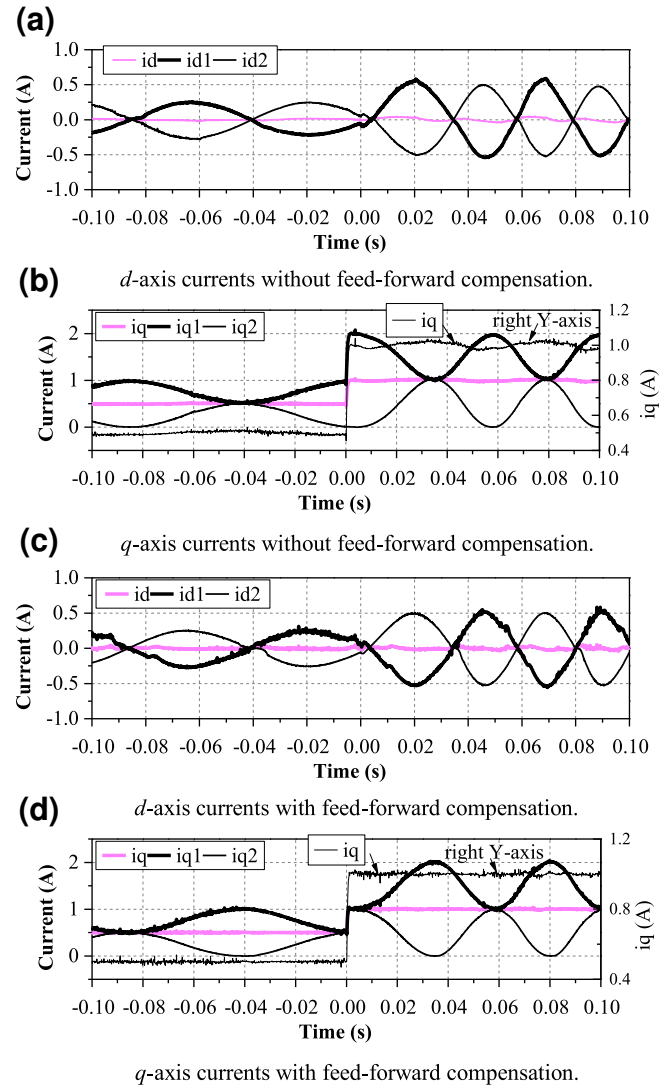


FIGURE 8 Measured step responses without/with feed-forward compensation

with feed-forward compensation are shown and compared in Figure 8. The dq -axis currents without and with feed-forward compensation are shown in Figure 8(a)–(d), respectively. As can be seen from Figure 8(b) and (d), the i_q response exhibits excellent performance in terms of step response and quick settling time in both cases with and without feed-forward compensation. However, i_q in Figure 8(d) has less oscillation in steady-state operation than that in Figure 8(b).

4.4 | Comparison of dynamic performance

The step response of the decoupling vector control with/without feed-forward compensation with one phase open is compared with the healthy DT-PMSM with VSD control in Figure 9. The i_q reference current is stepped from 0.5A to 1A at the time of 0s. It shows that their step responses are almost the same, which indicates that the decoupling fault-tolerant vector

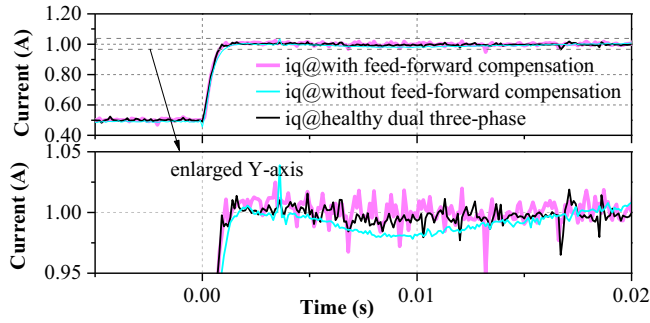


FIGURE 9 Comparison of the fault-tolerant control results with/without feed-forward compensation for DT-PMSM with one phase open and VSD control for the healthy DT-PMSM

control has similar performance as the VSD control for the healthy DT-PMSM. However, there is some oscillation in the i_q step response under control without feed-forward compensation, which resulted from the second-order harmonic current. The comparative results show that the proposed mathematical modelling of DT-PMSM is reasonable and correct.

5 | CONCLUSION

This study proposes a generic mathematical modelling and decoupling fault-tolerant vector control of DT-PMSM with one phase open, which accounts for the mutual coupling between two sets of three-phase windings and the second-order harmonic inductances. The general modelling methodology can also be extended to the dual three-phase machines or other multiphase machines with multiple phases open easily. Based on the proposed mathematical modelling, the permanent flux-linkage and current in the dq -frame become DC values. A proposed decoupling fault-tolerant vector control scheme with/without dedicated feed-forward voltage compensation is used in the experiments for the validation of mathematical modelling. With the dedicated feed-forward compensation, the second harmonic components in the dq -frame are well suppressed. The dynamic performance of the fault-tolerant control for the faulty DT-PMSM with one phase open is equivalent to that of the VSD control for healthy DT-PMSM, indicating the correctness of the proposed modelling.

NOMENCLATURE

F_ω F_β F_{z1}	Components in $\alpha\beta$ - $z_1z_2z_3$ frame
F_{z2} F_{z3}	F can be R , v , i , ψ_s or ψ_f , which represents to stator resistance, voltage, current, stator flux-linkage, or PM flux-linkage
$[F_{\alpha\beta z}]$	$[F_{\alpha\beta z}] = [F_\alpha \ F_\beta \ F_{z1} \ F_{z2} \ F_{z3}]^T$
$[F_{\alpha\beta}]$	$[F_\alpha \ F_\beta]^T$
F_{α_2} F_{β_2}	Components in $\alpha_2\beta_2$ -frame
$[F_{\alpha_2\beta_2}]$	$[F_{\alpha_2} \ F_{\beta_2}]^T$
$F_{d\beta}$ F_q	Components in dq -frame for dual three-phase PMSM
$[F_{dq}]$	$[F_d \ F_q]^T$

F_{d1} F_{q1}	Components in the dq -frame for the first set of three-phase windings
F_{d2} F_{q2}	Components in the dq -frame for the second set of three-phase windings
$[L_{\alpha\beta z}]$	Inductance matrix in $\alpha\beta$ - $z_1z_2z_3$ frame
$[R_{\alpha\beta z}]$	Resistance matrix in $\alpha\beta$ - $z_1z_2z_3$ frame
$[L_{\alpha\beta}]$	Inductance matrix in $\alpha\beta$ -frame
L_{z1}	Inductance in z_1 -axis
$[M_{\alpha\beta z1}]$	Mutual inductance matrix between $\alpha\beta$ -frame and z_1 -axis
$M_{z1\beta}$	Mutual inductance between β -axis and z_1 -axis
$[L_{\alpha_2\beta_2}]$	Inductance matrix in $\alpha_2\beta_2$ -frame
$[M_{\alpha_2\beta_2 z1}]$	Mutual inductance matrix between $\alpha_2\beta_2$ -frame and z_1 -axis
$[L_{dq}]$	Inductance matrix in dq -frame
$[M_{dqz1}]$	Mutual inductance matrix between dq -frame and z_1 -axis

ORCID

Yashan Hu  <https://orcid.org/0000-0001-6585-9017>

REFERENCES

- Gaeta, A., Scelba, G., Consoli, A.: Modeling and control of three-phase PMSMs under open-phase fault. *IEEE Trans. Ind. Appl.* 49(1), 74–83 (2013)
- Jiang, X., et. al.: Analysis of a dual-winding fault-tolerant permanent magnet machine drive for aerospace applications. *IEEE Trans. Magn.* 51(11), 1–4 (2015)
- Demir, Y., Aydin, M.: A novel dual three-phase permanent magnet synchronous motor with asymmetric stator winding. *IEEE Trans. Magn.* 52(7), 1–5 (2016)
- Jiang, X., et. al.: Electric drive system of dual-winding fault-tolerant permanent-magnet motor for aerospace applications. *IEEE Trans. Ind. Electron.* 62(12), 7322–7330 (2015)
- Barcaro, M., Bianchi, N., Magnussen, F.: Faulty operations of a PM fractional-slot machine with a dual three-phase winding. *IEEE Trans. Ind. Electron.* 58(9), 3825–3832 (2011)
- Wang, X., et. al.: Comprehensive diagnosis and tolerance strategies for electrical faults and sensor faults in dual three-phase PMSM drives. *IEEE Trans. Power Electron.* 34(7), 6669–6684 (2019)
- Liu, T. H., Fu, J. R., Lipo, T. A.: A strategy for improving reliability of field-oriented controlled induction motor drives. *IEEE Trans. Ind. Appl.* 29(5), 910–918 (1993)
- Zhao, Y. F., Lipo, T. A.: An approach to modeling and field-oriented control of a three phase induction machine with structural imbalance. *Proc. Appl. Power Electron. Conf.*, vol. 1, pp. 380–386. APEC, San Jose, CA (1996)
- Zhou, X., Sun, J., Li, H., Song, X.: High performance three-phase PMSM open-phase fault-tolerant method based on reference frame transformation. *IEEE Trans. Ind. Electron.* 66(10), 7571–7580 (2019)
- Zhou, X., et. al.: PMSM open-phase fault-tolerant control strategy based on four-leg inverter. *IEEE Trans. Power Electron.* 35(3), 2799–2808 (2020)
- Wang, X., et. al.: Diagnosis and tolerance of common electrical faults in T-type three-level inverters fed dual three-phase PMSM drives. *IEEE Trans. Power Electron.* 35(2), 1753–1769 (2020)
- Guo, Y., et. al.: Adaptive torque ripple suppression methods of three-phase PMSM during single-phase open-circuit fault-tolerant operation. *IEEE Trans. Ind. Appl.* 1–1 (2020)
- Hu, W., Ruan, C., Nian, H., Sun, D.: Simplified modulation scheme for open-end winding PMSM system with common DC bus under open-

- phase fault based on circulating current suppression. *IEEE Trans. Power Electron.* 35(1), 10–14 (2020)
14. Salem, A., Narimani, M.: A review on multiphase drives for automotive traction applications. *IEEE Trans. Transp. Electrification.* 5(4), 1329–1348 (2019)
 15. Melo, V. F. M. B., et al.: Fault tolerance performance of two hybrid six-phase drive systems under single-phase open-circuit fault operation. *IEEE Trans. Ind. Appl.* 55(3), 2973–2983 (2019)
 16. Eldeeb, H. M., et al.: Postfault full torque–speed exploitation of dual three-phase IPMSM drives. *IEEE Trans. Ind. Electron.* 66(9), 6746–6756 (2019)
 17. Hu, Y., Huang, S., et al.: Control of dual three-phase permanent magnet synchronous machine based on five-leg inverter. *IEEE Trans. Power Electron.* 34(11), 11071–11079 (2019)
 18. Ryu, H. M., Kim, J. W., Sul, S. K.: Synchronous-frame current control of multiphase synchronous motor under asymmetric fault condition due to open phases. *IEEE Trans. Ind. Appl.* 42(4), 1062–1070 (2006)
 19. Cheng, L., et al.: Implementation of postfault decoupling vector control and mitigation of current ripple for five-phase fault-tolerant PM machine under single-phase open-circuit fault. *IEEE Trans. Power Electron.* 33(10), 8623–8636 (2018)
 20. Kianinezhad, R., et al.: Modeling and control of six-phase symmetrical induction machine under fault condition due to open phases. *IEEE Trans. Ind. Electron.* 55(5), 1966–1977 (2008)
 21. Che, H. S., et al.: Fault-tolerant symmetrical six-phase induction motor drive based on feed-forward voltage compensation. In: *Proceedings of IECON 2019 - 45th Annual conference of the IEEE Industrial Electronics Society*, pp. 6212–6216. Lisbon, Portugal (2019)
 22. Shamsi-Nejad, M. A., et al.: Fault tolerant and minimum loss control of double-star synchronous machines under open phase conditions. *IEEE Trans. Ind. Electron.* 55(5), 1956–1965 (2008)
 23. Feng, G., et al.: Open-phase fault modeling and optimized fault-tolerant control of dual three-phase permanent magnet synchronous machines. *IEEE Trans. Power Electron.* 34(11), 11116–11127 (2019)
 24. Wang, X. L., et al.: Current-controlled multiphase slice permanent magnetic bearingless motors with open-circuited phases: Fault-tolerant controllability and its verification. *IEEE Trans. Ind. Electron.* 59(5), 2059–2072 (2012)
 25. Wang, W., et al.: Fault-tolerant control of dual three-phase permanent-magnet synchronous machine drives under open-phase faults. *IEEE Trans. Power Electron.* 32(3), 2052–2063 (2017)
 26. Zhou, C., et al.: Control strategy for dual three-phase PMSM based on reduced order mathematical model under fault condition due to open phases. *J. Eng.* 2018(13), 489–494 (2018)
 27. Hu, Y., Zhu, Z. Q., Odavic, M.: Comparison of two-individual current control and vector space decomposition control for dual three-phase PMSM. *IEEE Trans. Ind. Appl.* 53(5), 4483–4492 (2017)
 28. Hu, Y., Zhu, Z. Q., Odavic, M.: Comparative study of current control methods of asymmetric PM synchronous machine. 2016 XXII International conference on electrical machines (ICEM), pp. 982–988. Lausanne, Switzerland (2016)
 29. Zmood, D. N., Holmes, D. G.: Stationary frame current regulation of PWM inverters with zero steady-state error. *IEEE Trans. Power Electron.* 18(3), 814–822 (2003)
 30. Zhao, Y. F., Lipo, T. A.: Space vector PWM control of dual three-phase induction machine using vector space decomposition. *IEEE Trans. Ind. Appl.* 31(5), 1100–1109 (1995)
 31. Hu, Y., Zhu, Z. Q., Liu, K.: Current control for dual three-phase permanent magnet synchronous motors accounting for current unbalance and harmonics. *IEEE Trans. Emerg. Sel. Topics Power Electron.* 2(2), 272–284 (2014)
 32. Prieto, I. G., et al.: Field oriented control of multiphase drives with passive fault-tolerance. *IEEE Trans. Ind. Electron.* 67(9), 7228–7238 (2019)
 33. Zhao, Y. F., Lipo, T. A.: Modeling and control of a multi-phase induction machine with structural unbalance. Part I: Machine modeling and multi-dimensional current regulation. *IEEE Trans. Energy Convers.* 11(3), 570–577 (1996)
 34. Zhao, Y. F., Lipo, T. A.: Modeling and control of a multi-phase induction machine with structural unbalance. Part II: Field-oriented control and experimental verification. *IEEE Trans. Energy Convers.* 11(3), 578–584 (1996)
 35. Gebregergis, A., et al.: Evaluation of inductance in a permanent magnet synchronous motor. *Proceedings of IEEE international electric machines and drives conference*. pp. 1171–1176. Niagara Falls, ON, Canada. (2011)
 36. Kallio, S., et al.: Decoupled $d-q$ model of double-star interior-permanent-magnet synchronous machines. *IEEE Trans. Ind. Electron.* 60(6), 2486–2494 (2013)
 37. Baneira, F., et al.: Control strategy for multiphase drives with minimum losses in the full torque operation range under single open-phase fault. *IEEE Trans. Power Electron.* 32(8), 6275–6285 (2017)
 38. Blasko, V., Kaura, V., Niewiadomski, W.: Sampling of discontinuous voltage and current signals in electrical drives: A system approach. *IEEE Trans. Ind. Appl.* 34(5), 1123–1130 (1998)
 39. Fitzgerald, A. E., Kingsley, C., Umans, S. D.: *Electric Machinery*, 6th ed. McGraw-Hill, New York (2002)

How to cite this article: Hu Y, Zhu ZQ, Wu Z. Modelling and vector control of dual three-phase PMSM with one-phase open. *IET Electr. Power Appl.* 2021;15:847–860. <https://doi.org/10.1049/elp2.12064>

APPENDIX

1) Equations in abc -xyz frame

The mathematical modelling in the abc -xyz frame has been introduced in Section 2.1. In terms of electromagnetic torque, it can be calculated as the derivative of the stored magnetic coenergy W_c with respect to a small displacement [39]. In the same way, the torque for the faulty dual three-phase PMSM can be expressed as:

$$T_e = \frac{\partial W_c}{\partial \Omega} = \frac{p}{2} [i_s]^T \frac{\partial [L_s]}{\partial \theta} [i_s] + p [i_s]^T \frac{\partial [w_f]}{\partial \theta} \quad (A1)$$

where p is the number of pole pairs. As can be seen from Equation (A1), the torque includes two parts, the first part of Equation (A1) is the reluctance torque, and the second part of Equation (A1) is PM torque.

2) Equations in $\alpha\beta$ - $z_1z_2z_3$ subplanes

The inductance matrix in the $\alpha\beta$ -frame can be expressed as:

$$\begin{aligned} [L_{\alpha\beta}] &= \left(\frac{L_{d1} + L_{q1}}{2} \right) I_2 + \left(\frac{L_{d1} - L_{q1}}{2} \right) \begin{bmatrix} \cos(2\theta) & \sin(2\theta) \\ \sin(2\theta)/2 & -\cos(2\theta) \end{bmatrix} + \\ & \left(\frac{M_{d12} + M_{q12}}{2} \right) I_2 + \left(\frac{M_{d12} - M_{q12}}{2} \right) \begin{bmatrix} \cos(2\theta) & \sin(2\theta) \\ \sin(2\theta)/2 & 0 \end{bmatrix} \end{aligned} \quad (A2)$$

where

$$L_{d1} = L_{d2} = L_{sl} + L_{dqavg} + \frac{M_{dqavg}}{2} + \frac{(L_{dqdiff} + 2M_{dqdiff})}{2} \quad (A3)$$

$$L_{q1} = L_{q2} = L_{sl} + L_{dqavg} + \frac{M_{dqavg}}{2} - \frac{(L_{dqdiff} + 2M_{dqdiff})}{2} \quad (A4)$$

$$M_{d21} = M_{d12} = 3(M_{dq12avg} + M_{dq12diff})/2 \quad (A5)$$

$$M_{q21} = M_{q12} = 3(M_{dq12avg} - M_{dq12diff})/2 \quad (A6)$$

$$I_2 = \begin{bmatrix} 1 & 0 \\ 0 & 1 \end{bmatrix} \quad (A7)$$

The mutual inductance matrix between $\alpha\beta$ -frame and z_1 -axis can be expressed as:

$$[M_{\alpha\beta z_1}] = \left(\frac{(L_{d1} - L_{q1})}{2} - \frac{(M_{d12} - M_{q12})}{2} \right) \begin{bmatrix} 0 \\ \sin(2\theta) \end{bmatrix} \quad (A8)$$

The self-inductance in z_1 -axis is:

$$L_{z1} = \left(\frac{L_{d1} + L_{q1}}{2} \right) + \left(\frac{L_{d1} - L_{q1}}{2} \right) \cos(2\theta) - \left(\frac{M_{d12} + M_{q12}}{2} \right) - \left(\frac{M_{d12} - M_{q12}}{2} \right) \cos(2\theta) \quad (A9)$$

The mutual inductance $M_{z1\beta}$ can be expressed as:

$$M_{z1\beta} = \left(\left(\frac{L_{d1} - L_{q1}}{2} \right) - \left(\frac{M_{d12} - M_{q12}}{2} \right) \right) \sin(2\theta) \quad (A10)$$

By the introduction of matrix $[B]$, the inductance matrix in $\alpha_2\beta_2$ -frame can be expressed as:

$$[L_{\alpha_2\beta_2}] = [B][L_{\alpha\beta}][B]^{-1} = \left(\frac{L_{d1} + L_{q1}}{2} \right) I_2 + \left(\frac{L_{d1} - L_{q1}}{2} \right) \begin{bmatrix} \cos(2\theta) & \sin(2\theta)/2 \\ \sin(2\theta) & -\cos(2\theta) \end{bmatrix} + \left(\frac{M_{d12} + M_{q12}}{2} \right) I_2 + \left(\frac{M_{d12} - M_{q12}}{2} \right) \begin{bmatrix} \cos(2\theta) & \sin(2\theta)/2 \\ \sin(2\theta) & 0 \end{bmatrix} \quad (A11)$$

$$[M_{\alpha_2\beta_2 z_1}] = [B][M_{\alpha\beta z_1}] = \left(\left(\frac{L_{d1} - L_{q1}}{2} \right) - \left(\frac{M_{d12} - M_{q12}}{2} \right) \right) \begin{bmatrix} 0 \\ \sin(2\theta) \end{bmatrix} \quad (A12)$$

Since

$$[i_s] = [T_5]^{-1} [i_{\alpha\beta z}] \quad (A13)$$

$$[L_s] = [T_5]^{-1} [L_{\alpha\beta z}] [T_5] \quad (A14)$$

$$[\psi_f] = [T_5]^{-1} [\psi_{f\alpha\beta z}] \quad (A15)$$

Substituting Equations (A13), (A14) and (A15) into Equation (A1) and after simplification, the torque calculated in $\alpha\beta$ - $z_1z_2z_3$, subplanes can be expressed in Equation (A16):

$$T_e = \frac{p}{2} \left([i_{\alpha\beta z}]^T [M_5] \frac{\partial [L_{\alpha\beta z}]}{\partial \theta} [i_{\alpha\beta z}] \right) + p \left([i_{\alpha\beta z}]^T [M_5] \frac{\partial [\psi_{f\alpha\beta z}]}{\partial \theta} \right) \quad (A16)$$

where $[M_5]$ is expressed in Equation (A17).

$$[M_5] = ([T_5]^{-1})^T [T_5]^{-1} \quad (A17)$$

Neglecting reluctance torque, the Equation (A16) can be rewritten as:

$$T_e = 3p \left([i_{\alpha\beta}]^T [B] \frac{\partial [\psi_{f\alpha\beta}]}{\partial \theta} \right) \quad (A18)$$

Since

$$[i_{\alpha\beta}]^T = ([B]^{-1} [i_{\alpha_2\beta_2}])^T = [i_{\alpha_2\beta_2}]^T ([B]^{-1})^T \quad (A19)$$

$$[\psi_{s\alpha_2\beta_2}] = [B] [\psi_{s\alpha\beta}] \quad (A20)$$

Equation (A18) can be rewritten as:

$$T_e = 3p \left([i_{\alpha_2\beta_2}]^T [B]^{-1} \frac{\partial ([\psi_{f\alpha_2\beta_2}])}{\partial \theta} \right) \quad (A21)$$

3) Equations in dq -frame

The inductances in dq -frame can be expressed as:

$$[L_{dq}] = \begin{bmatrix} L_d^{equ} & 0 \\ 0 & L_q^{equ} \end{bmatrix} + \quad (\text{A22})$$

$$\frac{1}{2} \left(L_{dq-ac1} - L_{dq-ac2} \cos(2\theta) \right) [M(\theta)]$$

$$L_d^{equ} = L_{d1} + M_{d12} \quad (\text{A23})$$

$$L_q^{equ} = L_{q1} + M_{q12} \quad (\text{A24})$$

$$L_{dq-ac1} = (L_{d1} + L_{q1})/2 - (M_{d12} + M_{q12})/2 \quad (\text{A25})$$

$$L_{dq-ac2} = (L_{d1} - L_{q1})/2 - (M_{d12} - M_{q12})/2 \quad (\text{A26})$$

The mutual inductance matrix between dq -frame and z_1 -axis can be expressed as:

$$[M_{dqz1}] = M_{dqz1-ac} \sin(2\theta) \begin{bmatrix} \sin(\theta) \\ \cos(\theta) \end{bmatrix} \quad (\text{A27})$$

where

$$M_{dqz1-ac} = L_{dq-ac2} \quad (\text{A28})$$

If the second harmonic inductance is neglected, L_{dq-ac2} and $M_{dqz1-ac}$ will be zero. Since,

$$\begin{aligned} [i_{\alpha\beta 2}]^T &= ([T_{dq}]^{-1} [i_{dq}])^T = [i_{dq}]^T \cdot ([T_{dq}]^{-1})^T \\ [\psi_{f\alpha\beta 2}] &= [T_{dq}]^{-1} [\psi_{fdq}] \end{aligned} \quad (\text{A29})$$

Neglecting the reluctance torque, Equation (A21) can be rewritten as:

$$T_e = 3p [i_{dq}]^T ([T_{dq}]^{-1})^T [B]^{-1} \frac{\partial ([T_{dq}]^{-1} [\psi_{fdq}])}{\partial \theta} \quad (\text{A30})$$

Assuming $[\psi_{fdq}]$ is constant, Equation (A30) can be simplified as:

$$\begin{aligned} T_e &= 3p [i_{dq}]^T ([T_{dq}]^{-1})^T [B]^{-1} \frac{\partial ([T_{dq}]^{-1} [\psi_{fdq}])}{\partial \theta} \\ &= p \left([i_{dq}]^T \begin{bmatrix} 0 & -3 \\ 3 & 0 \end{bmatrix} [\psi_{fdq}] \right) = 3p (-i_d \psi_{fq} + i_q \psi_{fd}) \end{aligned} \quad (\text{A31})$$